THE JOURNAL OF PHYSICAL CHEMISTRY Letters

Letter

Cite This: J. Phys. Chem. Lett. 2019, 10, 1361−1367

pubs.acs.org/JPCL

Making Sense of Coulomb Explosion Imaging

Itamar Luzon,[†,¶] Ester Livshits,[‡,¶] Krishnendu Gope,[†] Roi Baer,[*,‡] and Daniel Strasser[*,†]

[†]Institute of Chemistry, The Hebrew University of Jerusalem, Jerusalem 91904, Israel

[‡]Fritz Haber Center for Molecular Dynamics and the Institute of Chemistry, The Hebrew University of Jerusalem, Jerusalem 91904, Israel

Supporting Information

ABSTRACT: A multifaceted agreement between ab initio theoretical predictions and experimental measurements, including branching ratios, channel-specific kinetic energy release, and three-body momentum correlation spectra, leads to the identification of new mechanisms in Coulomb-explosion (CE) induced two- and three-body breakup processes in methanol. These identified mechanisms include direct nonadiabatic Coulomb explosion responsible for CO bond-breaking, a long-range " inverse harpooning" dominating the production of H_2^+ + $HCOH^+$, a transient proton migration leading to surprising energy partitioning in three-body fragmentation and other complex dynamics forming products such as H_2O^+ and H_3^+. These mechanisms provide general concepts that should be useful for analyzing future time-resolved Coulomb explosion imaging of methanol as well as other molecular systems. These advances are enabled by a combination of recently developed experimental and computational techniques, using weak ultrafast EUV pulses to initiate the CE and a high-level quantum chemistry approach to follow the resulting field-free nonadiabatic molecular dynamics.

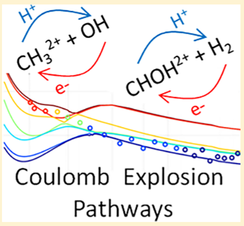

Time-resolved imaging of dynamical events in complex molecular processes is a grand challenge of ultrafast spectroscopy still beyond our reach. One of the ways for achieving this goal involves the use of ultrafast laser pulses to induce a violent Coulomb explosion (CE) in a molecule and then to measure by coincidence-imaging techniques the correlated momenta of the ejected cations.[1−3] It was assumed that the measured momentum correlations could be interpreted in sufficient detail and reliability to allow determination of the instantaneous molecular structure prevailing just before the split-femtosecond occurrence of the explosion.[4,5] However, despite significant advances in the CE technique, interpretation of Coulomb explosion imaging (CEI) data is still limited. Ideally, one would like to have a "button" pressed at zero time that instantaneously pumps sufficient energy into the molecular system for Coulomb-explosion to occur simetime later. One would then be able to use molecular dynamics to analyze the ensuing "trajectories", thereby allowing a detailed interpretation of the experiment. However, meeting this ideal is complicated because typical CEI experiments use low-frequency high-intensity laser pulses to ignite the explosion. These pulses die out eventually, but during their operation the molecule absorbs their energy through complex multiphoton processes, and by undergoing complicated field-dressed multielectron molecular dynamics, including structural rearrangements on the field-dressed states,[6,7] molecular alignment, and bond softening.[8] It is impossible to follow these nonlinear effects using existing computational algorithms, except in very small molecules such as H_2 or D_2.[9−12] Hence, by the time the pulses have died off and field-free dynamics finally takes over, the molecular configuration has changed too much to allow for a reliable and detailed interpretation of the results.

But the problem is not only experimental, it is also computational. Even under field-free conditions, the electron−nuclear dynamics is an exceptionally complicated process in polyatomic systems due to their inherent multireference character, which complicates the use of single-reference approaches such as time-dependent density functional theory[13,14] Green's function methods,[15] and coupled-cluster approaches.[16−18] Complications remain even when using complete active space multiconfigurational self-consistent field[19] theory due to the inaccurate treatment of dynamical electron correlation in this approach. The combination of CASSCF with second-order perturbation theory, dubbed CASPT2[20] seems to overcome all these problems but was not used for dynamics until recently, since energy and wave function gradients (force and nonadiabatic couplings) were not implemented due to complications in deriving error-free theoretical expressions for them.

In this Article, using a novel combination of experimental and computational approaches, we present a breakthrough development toward time-resolved CEI, addressing both of the above-described challenges. The first element in the combination is the use of high-order harmonic generation (HHG)[21−24] to produce ultrafast EUV pulses inducing instantaneous single-photon double ionization.[25] Thus, dications are formed in the Franck−Condon (FC) geometry of its time-resolved neutral parent.[26,27] The second element is the use of a highly accurate nonadiabatic *ab initio* molecular dynamics (NA-AIMD) method for interpretation of the experimental results. This development relies on the recently developed CASPT2

Received: February 27, 2019
Accepted: March 6, 2019
Published: March 6, 2019

DOI: 10.1021/acs.jpclett.9b00576

gradients, which is unique in the BAGEL code.[28,29] To demonstrate our novel method, we applied it to the doubly ionized methanol, recently studied in the context of CEI by several groups.[26,30,31] While intense laser CEI of methanol was shown to depend on the exact laser parameters,[7] we discovered that the single-photon approach allows for a remarkable matching between the experimental and *ab initio* product branching ratios and kinetic energy release (KER) spectra. In particular, theory-inspired experiments allow for the first time to directly compare detailed experimental and *ab initio* momenta correlations in three-body dication breakup. Moreover, the availability of NA-AIMD trajectories offers an unprecedented detailed interpretation of a variety of nonadiabatic processes leading to the observed two- and three-body CE product distributions.

The experimental measurements yield asymptotic cation momenta and branching ratios, which give the relative yields of both two- and three-body CE channels. Five two-body CE channels are observed, and their measured branching ratios are compared to *ab initio* predicted yields in Figure 1. The predominant two-body channels in the experimental data are the CO bond-breaking CH_3^+ + OH^+ and the trihydrogen cation ejection H_3^+ + COH^+. Proton or H_2^+ ejection, as well as the intriguing proton migration channel producing CH_2^+ + H_2O^+, exhibit lower yields.

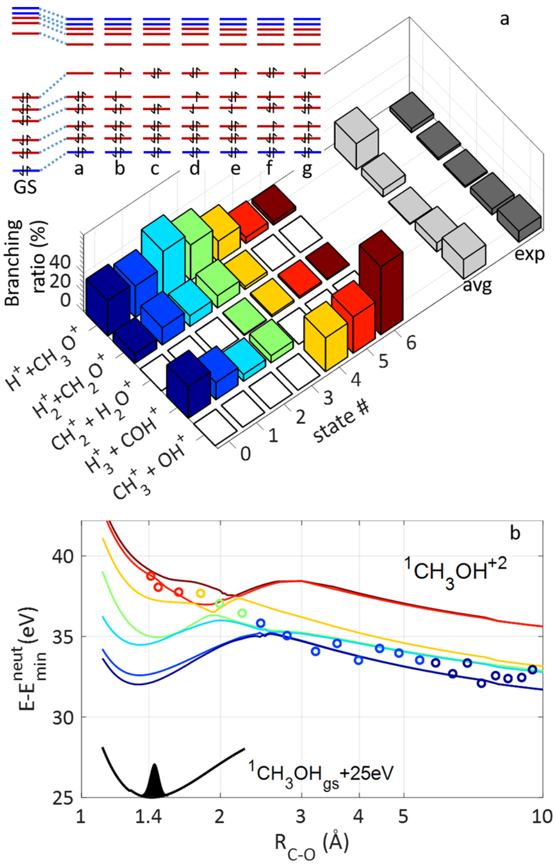

Figure 1. (a) Experimental branching ratios for the two-body CE channels (exp) are compared to the calculated ratios (avg). The average is taken over the product distributions obtained from ~700 trajectories starting from the seven lowest adiabatic dication states (numbered 0−6). The inset describes the electronic diabatic configurations dominating the neutral ground state and the seven lowest adiabatic dication states (see text for details). (b) Adiabatic potential curves for the CO bond-breaking channel $CH_3OH^{2+} \rightarrow CH_3^+ + OH^+$. The empty circles depict the energies and bond lengths along a typical CO bond-breaking nonadiabatic trajectory at 5.1 fs intervals.

Theoretically, the seven lowest adiabatic dication states are considered, these are dominated by the diabatic configurations corresponding to 2e removal from the neutral ground state, shown in the Figure 1a inset. Adiabatic states 0, 1, and 2 are dominated by diabatic configurations a, b, and c, respectively; state 3 is mainly a linear combination of c and d, and linear combinations of configurations d−g form state 4−6. In the FC region, Mulliken charges of the methyl and hydroxyl groups of these dication states are about +1.5e and +0.5e, respectively. Therefore, for the CO bond-breaking CE channel to occur, a +0.5e charge transfer that forms a potential barrier must take place. As shown in Figure 1b, the barrier appears at R_{CO} ~ 2.8 Å in all seven adiabatic states. Nevertheless, a dication initiated on one of the high excited states can break the CO bond via a series of nonadiabatic transitions. The open circles in Figure 1b show 5.1 fs time steps of a typical CO bond-breaking trajectory, which is initiated on the fifth excited state, rapidly reaching the dication ground state. The required charge transfer can be also mediated by proton migration, similarly occurring on the high excited states. However, for states 0−3 in which CO bond-breaking is effectively blocked, more complex CE dynamics lead to formation of the trihydrogen H_3^+ cation. Thus, even single-photon CE requires considering dynamics on a wide range of excited states. As shown in Figure 1a the average computed branching ratios of these three channels exhibit quantitative agreement with the experimental data. However, *ab initio*-predicted yields of the proton and H_2^+ ejection channels overestimate the final experimental branching ratios.

To obtain mechanistic insight and critically test *ab initio* computational models, it is important to directly compare not only branching ratios but also dynamical observables, such as channel resolved KER spectra. The left column panels of Figure 2 show the interfragment velocity as a function of the time derivative of the interfragment distance, computed as a function of time for selected trajectories, reflecting the different dynamics leading to the five two-body CE channels. The instantaneous electronic state is encoded in the color. Trajectory color changes as a function of time evolution represent surface hopping events. For each channel, the asymptotic interfragment velocities are used to derive the KER spectra. Within the statistics of the computed trajectories, different initial electronic states exhibit similar KER distributions as can be seen from the KER spectra that are color labeled by the simulated initial electronic excitation. Thus, significant few electronvolt differences in the initial electronic excitation are largely transferred to product internal electronic as well as ro-vibrational excitation rather than to the KER. The right column panels of Figure 2 quantitatively compare the average computed KER spectra with the measured data for the five possible two-body CE channels, normalized to the total double ionization yield.

CH_3^+ + OH^+ trajectories show strictly positive interfragment velocities, hence indicating a direct CE, on a ~40 fs time scale, facilitated by the strong adiabatic coupling. Returning to the KER distribution of the CO bond-breaking channel, average theoretical and experimental spectra in Figure 2 show a large degree of agreement, with both distributions peaking at ~6 eV. Due to the strong nonadiabatic coupling discussed earlier, the

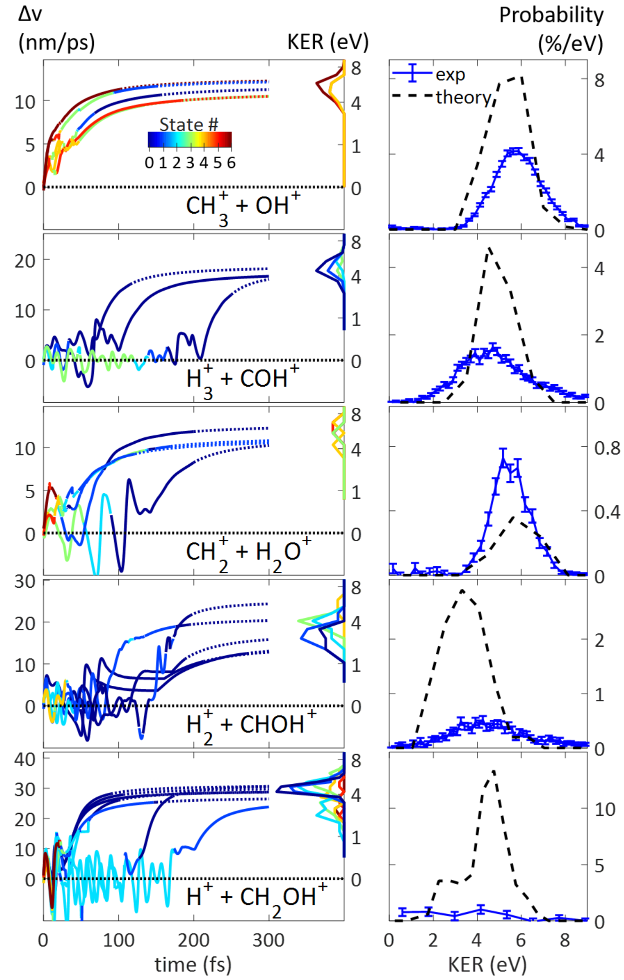

Figure 2. Left column panels: interfragment velocities in typical NA-AIMD trajectories as a function of time for different two-body CE channels. The instantaneous state along each trajectory is color coded, reflecting surface hopping during the time evolution. The KER distributions for different initial states are projected on the right axis. Right column panels: quantitative comparison of experimental KER spectra with the average calculated results.

dissociation occurs on a diabatic potential that is highlighted by the potential along a typical NA-AIMD trajectory shown by open circles in Figure 1b. In such prompt dissociation on a strongly repulsive potential, the KER can be expected to reflect the initial instantaneous FC geometry. However, as the trajectories simulated here sample only the very narrow FC region, corresponding to the initial experimental temperature of 300 K, it is difficult to report an explicit correlation between KER and initial geometry. CO bond-breaking by proton migration leading to the final CH_2^+ + H_2O^+ channel is also initiated on the higher dication states (3−6). Nevertheless, the CE mechanism that transfers a proton from the methyl to the hydroxyl group develops on a longer time scale, as indicated by the oscillating interfragment velocities. The dissociation time varies, typically dissociating after 50−200 fs (see Figure 2), in which the CO bond completes several vibrations before bond cleavage. Although these longer time scales can allow for energy dissipation into internal degrees of freedom, both experimental and theoretical spectra peak at high ∼5.5 eV, showing once again an impressive agreement. When the CO bond does not break, the dication can relax by ejection of a light H_n^+ cation. The highest experimental yield is the H_3^+ + COH^+ with both experimental and computed KER distributions peaking at lower ∼4.3 eV KER (see Figure 2). The lower KER can be assigned to the lower initial electronic excitation (states 0−3), as well as to the increased dissipation into the other degrees of freedom as H_3^+ formation requires significant structural rearrangement. This intriguing product channel has been extensively studied using many ionization methods.[32,33] Similarly to previous AIMD studies on the dication ground state,[30,31,33,34]typical NA-AIMD trajectories resulting in H_3^+ formationa exhibit a roaming neutral H_2 that eventually plucks the last proton connected to C, at which point the vibrationally hot H_3^+ explodes away from the COH^+ cation. Consequently, the interfragment velocity in H_3^+ forming trajectories exhibit extended oscillations before dissociation takes place in agreement with time scales reported by time-resolved intense field measurements.[30,33,35]

Returning to the H^+ and H_2^+ products, we see in Figure 2 that the simulated trajectories of both channels exhibit significant time delays before dissociation, sometimes up to 250 fs. Furthermore, as shown already in Figure 1a, the computed proton and H_2^+ ejection trajectories overestimate their quantitative contribution to the coincidence imaging data. Nevertheless, their computed KER spectra are broad, in qualitative agreement with the experimental KER range. In the case of the $CHOH^+$ + H_2^+ channel, the computed time-resolved interfragment velocities reveal a remarkable and surprising fragmentation mechanism. In these trajectories, dissociation does not lead immediately to the characteristic rapid acceleration due to the long-range Coulomb repulsion displayed by other channels. CE is preceded by a long ∼100 fs stage of deceleration, reflecting attraction between the nearly separated products. Mulliken charge analysis confirms that at this stage a long-range charge transfer occurs. The typical mechanism is as follows: after ∼50−100 fs, an H_2^+ fragment starts separating and then during the separation, the hole located at the H_2^+ fragment is back transferred to the $CHOH^+$ group, resulting in deceleration. At this stage both charges are localized on the $CHOH^{2+}$ fragment that attracts the still separating neutral H_2. After ∼150 fs at interfragment distances as high as 6 Å, trajectories leading to $CHOH^+$ + H_2^+ undergo a long-range adiabatic charge transfer, clearly reflected in the rapid acceleration by the long-range Coulomb repulsion. This intricate mechanism, which can be described as an "inverse harpooning" mechanism,[36] results in a broad KER spectrum in both theoretical and experimental results.

The experimental error in the proton ejection channel makes it difficult to compare the shapes of the computed and experimental KER spectra. Nevertheless, the H_2^+ ejection channel data suggest that the low KER events are those missing from the experimental measurement. This, along with the long tail of dissociation delays suggests that sequential dissociation, at times beyond the present calculation, could result in neutral products, which cannot be directly detected in the experiment.

In search of the theoretically predicted H^+ and H_2^+ channels, the theoretical result inspired an experimental effort to observe "hidden" neutral products ejected during CE. Fortunately, our present HHG pulse produces vanishing triple-ionization yields. It is therefore possible to assume that all coincident $A^+ + B^+$ products of methanol for which $m_A + m_B < 32$ amu are accompanied by a "hidden" neutral fragment associated with the missing mass. Furthermore, with the advent of high resolution fragment imaging, it is possible to extract also the

DOI: 10.1021/acs.jpclett.9b00576
J. Phys. Chem. Lett. 2019, 10, 1361−1367

velocity vector of the "hidden" neutral product, based on the recoil of the center of mass of the "visible" cations. Figure 3 compares measured and calculated two- and three-body channel branching ratios. Clearly, the missing contributions of computed two-body proton and H_2^+ ejection are found in the experimental excess in three-body branching ratios, particularly toward $CHOH^+ + H^+ + H_2$ and $CHOH^+ + H_2^+ + H$, which are extremely rare in the computed trajectories. These three-body events that comprise over 50% of the measured CE data can result from sequential dissociation of electronically excited products indicated by the asymptotic electronic excitation presented in Figure 2. Furthermore, an additional mechanism for three body CE could be due to sequential fragmentation of the computed ~16% neutral H and H_2 ejection from the dication within the 300 fs trajectory time limit.

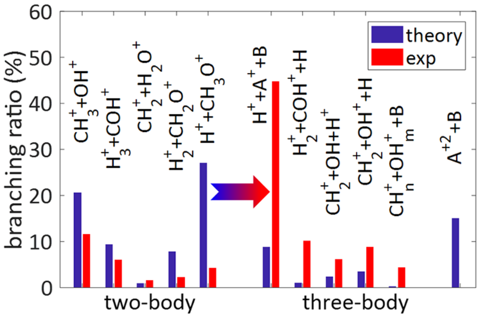

Figure 3. Branching ratios for all two- and three-body CE channels, directly comparing theoretical and experimental results.

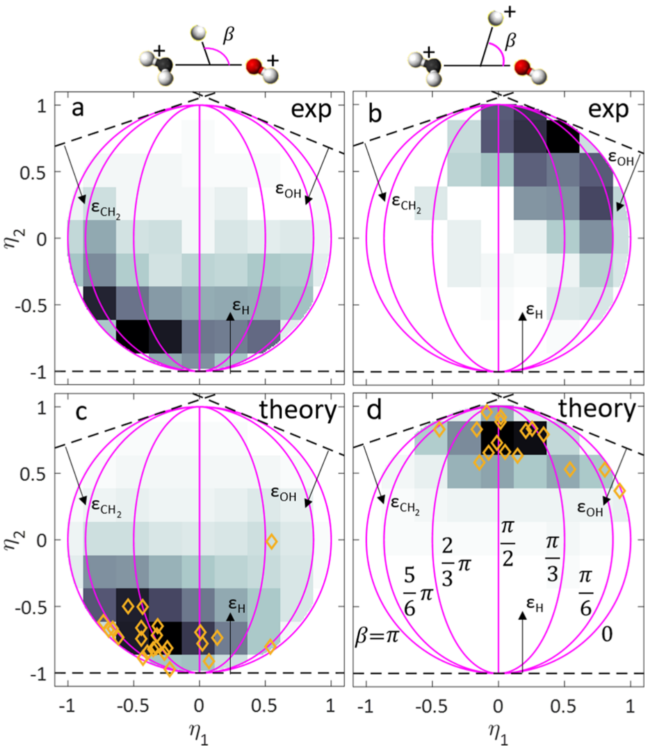

Figure 4. Dalitz plots comparing the experimental (a, b) and ab initio (c, d) three-body momentum correlations. Left and right panels, respectively, present the $CH_2^+ + OH^+ + H$, and $CH_2^+ + OH + H^+$ channels. Diamond markers indicate individual NA-AIMD trajectories, while the gray scale shows the simulated experimental response.

It is valuable to scrutinize not only the branching ratios but also the three-body correlations of channels that are predicated by the NA-AIMD trajectories. For example, CO bond-breaking is accompanied either by ejection of a neutral H or by a charged proton fragment. Both channels are found with few percent branching ratios in both theoretical and experimental data. We use the Dalitz plot representation of three-body momentum correlations for directly comparing measured experimental data with simulated three-body fragmentation trajectories. Dalitz plot coordinates were originally developed and used to present correlations, beyond the trivial correlations due to energy and momentum conservation, in unimolecular decays into three equal masses.[37−39] Here, the original coordinates developed by Dalitz are generalized for any three masses, where a random uncorrelated three-body fragmentation that obeys momentum conservation appears as a uniform distribution confined by a unit circle in the (η_1, η_2) plane.[37] The explicit mass scaled η_1, η_2 equations are given in the Supporting Information.

Parts a and b of Figure 4 show the experimentally measured Dalitz plots for the three-body CO bond-breaking channels, accompanied respectively by ejection of a neutral H or a proton. The η_2 coordinate is defined as $2\varepsilon_H - 1$, where ε_H is the fraction of the total KER carried away by the H fragment divided by the maximal fraction allowed by momentum conservation. For convenience, axes corresponding to the KER fractions carried by each fragment are labeled on the Dalitz plots in Figure 4 as ε_H, ε_{OH}, and ε_{CH_2}. The charged proton fragments that exhibit high η_2 values thus carry higher ε_H compared with neutral H fragments, as can be expected considering the strong Coulombic repulsion. Nevertheless, neutral fragments also exhibit surprising probability to carry away as much as half of the maximal possible kinetic energy, in both cases of neutral H and OH fragments. Dalitz plot longitude lines indicate fragmentation geometries with equal Jacobi angle β of the H fragment velocity relative to the CH_2−OH axis, where $\beta = 0$ and $\beta = \pi$ correspond to a colinear fragmentation, with H ejected in the direction of the OH or CH_2, respectively. Neutral H fragments are observed to be ejected toward the CH_2^+ product, reflecting the methanol ground state geometry. However, proton ejection exhibits an opposite trend that cannot be understood in simple terms of the molecular structure. Clearly, successful theoretical description of three-body correlations is a valuable key for interpretation of CEI measurements. Parts c and d of Figure 4 show the simulated Dalitz plots for the $CH_2^+ + OH^+ + H$ and $CH_2^+ + OH + H^+$, respectively. Diamond markers indicate individual computed trajectories, while the gray scale distributionis obtained by a Monte Carlo simulation of the experimental response, assuming isotropic orientation of the dissociation plane. This in agreement with the isotropic angular distributions, measured for all two-body channels.[26] The remarkable success of the CASPT2 level NA-AIMD trajectory calculations in reproducing the measured three-body correlations allows making sense of the CE dynamics by identifying several underlying mechanisms, for which selected movies are provided in the Supporting Information.

For the $CH_2^+ + OH^+ + H$ channel, typical NA-AIMD trajectories begin with the immediate cleavage of the CO bond, where ejection of a neutral H from the methyl cation follows within up to ~250 fs. These dynamics do not involve significant structural rearrangement, accordingly the measured final momenta correlations reflect the neutral CH_3OH structure. Computed trajectories with concerted three body breakup within ∼70 fs exhibit particularly fast neutral H fragments, due to the transient charge transfer between H and OH fragments during the dissociation.

For the CH_2^+ + OH + H^+ channel, typical NA-AIMD trajectories exhibit proton motion from the carbon toward the oxygen, resulting in the breaking of both bonds within ∼100 fs. This structural rearrangement of the dication away from the FC geometry, is reflected in the bias toward $\beta \ll \pi/2$ in both computed and experimental data. Furthermore, NA-AIMD trajectories provide mechanistic insight also for CE depositing surprisingly high KER to the neutral OH fragment: A sequential mechanism of proton migration and dissociation into CH_2^+ + H_2O^+, quickly followed by H^+ ejection, allows transient acceleration of the heavy oxygen mass. Thus, transient proton migration results in a counterintuitive KER partitioning between neutral and charged CE products.

CE of polyatomic molecules exhibits rich complex dynamics which interpretation requires successful *ab initio* description of the underlying mechanisms. The present study demonstrates that single-photon CEI of a polyatomic system can be quantitatively modeled and understood by considering nonadiabatic *ab initio* dynamics on the ground and excited dication states, unperturbed by the low-field ultrafast EUV pulse. The successful description of the measured channel branching ratios, KER spectra and three-body Dalitz plot correlations, allows describing and assigning the underlying CEI mechanisms. CE dynamics exhibit ultrafast transient charge migration, resulting in surprising and nontrivial product correlations. Long-range adiabatic charge exchange or " inverse harpooning" results in a delayed Coulomb explosion of nearly dissociated H_2 + $HCOH^{2+}$ systems. Concerted ejection of neutral and cationic fragments, as well as transient proton migration, result in surprisingly high KER deposited in previously overlooked neutral products of Coulomb explosion. Nevertheless, the presented CASPT2 level NA-AIMD trajectory calculations, uniquely enabled by the BAGEL code, allow making sense of the observed CE dynamics leading to the different final channels. On one hand, final channels such as the prompt CO bond-breaking on a diabatic potential, with or without ejection of a neutral H, can directly reflect the instantaneous structure of the parent neutral species in the observed KER spectra and three body Dalitz plot correlations. On the other hand, branching ratios toward final channels such as H_3^+ + COH^+, CH_2^+ + H_2O^+, or CH_2^+ + OH + H^+ that involve significant structural rearrangement on the dication can be expected to be sensitive to the parent neutral structure at the instance of single-photon double ionization. The critical comparison between experiment and theory, made possible by the low field single-photon double ionization using ultrafast HHG pulses with CASPT2 level NA-AIMD trajectory computations, opens opportunities for time-resolved investigations. In particular, the new surprising mechanisms described in the present study for the relatively simple methanol molecule are expected to be ubiquitous in molecular and macromolecular systems, multiply ionized due to all forms of EUV and X-ray radiation damage.[40,41]

The single-photon CEI experimental setup has been described earlier.[26] In brief, ultrafast EUV pulses are generated using HHG by a 2.1 mJ near IR laser pulse,[42] focused in a semi-infinite neon gas cell.[43] The low intensity EUV pulses are spatially filtered from the near-IR that have higher divergence.[44] At the center of home built 3D coincidence imaging spectrometer, the EUV pulse ionizes a skimmed effusive beam of methanol, where the cationic products are accelerated toward a time and position sensitive detector.[26,45] Low count rate and center of mass (CM) momentum conservation are used to suppress random coincidence cation signal due to dissociative ionization of two different parent molecules. Any residual contributions from random coincidence are estimated and subtracted on the basis of the measured single cation event probabilities. Further details of the three-body data analysis are provided in the Supporting Information.

For the NA-AIMD trajectory computations, we have generated 100 random configurations of methanol (geometries and velocities) from a 300 K AIMD trajectory of neutral methanol calculated at the CASSCF level using the MOLCAS package[46] at the (12e,10o)/aug-cc-pVTZ active space/basis-set level. Each of the 100 configurations was used for initiating a nonadiabatic molecular dynamics calculation of the methanol dication in each one of the seven lowest-lying dicationic electronic excited states. This generated 700 trajectories altogether. The ensuing nonadiabatic dynamics was approximated using surface-hopping molecular dynamics trajectories[47] generated at the XMS-CASPT2/(8e,8o)/aug-cc-pVDZ/density-fitting level using the BAGEL electronic structure package[29] within the so-called "left SS-SR" right contraction scheme[48] used for internally contracted basis functions in CASPT2 where a vertical shift set to $0.2E_h$ was used. The BAGEL code was interfaced with a modified version Newton-X (v1.4.0) program[49] for carrying out the surface hopping dynamics.[28] To facilitate the trajectory calculations, the system in adiabatic state n is allowed to hop *only* to the state m nearest in energy above or below it (i.e., we neglect the nonadiabatic coupling terms τ_{nm} unless $|n - m| = 1$). We modified the way Newton-X interfaces with the BAGEL code to enable this approximation. The time step for the NA-AIMD trajectories is 0.3 fs. The *ab initio* dynamics are followed for at most 300 fs or until the interfragment velocities are observed to reach an asymptotic monotonic behavior. At this stage, the effect of the residual long-range Coulomb repulsion on the final velocities is taken into account using the classical equations of motion applied to the center of masses of the resulting cationic fragments.

■ ASSOCIATED CONTENT

Ⓢ Supporting Information

The Supporting Information is available free of charge on the ACS Publications website at DOI: 10.1021/acs.jpclett.9b00576.

Selected nonadiabatic AIMD trajectory movies, showing the different CE mechanisms described in the manuscript (movie descriptions in the pdf Supporting Information file) (ZIP)

Detailed description of the three-body data analysis proceedures as well as the computational methods (PDF)

■ AUTHOR INFORMATION

Corresponding Authors

*E-mail: roi.baer@huji.ac.il.
*E-mail: strasser@huji.ac.il.

ORCID

Roi Baer: 0000-0001-8432-1925

Daniel Strasser: 0000-0002-9000-3816

Author Contributions

¶These authors contributed equally.

Notes

The authors declare no competing financial interest.

■ ACKNOWLEDGMENTS

We acknowledge funding from the ERC grant #306783 and ISF grants #1369/17 189/14 as well as funding from the Wolfson foundation. E.L. and R.B. gratefully thank Drs. Toru Shiozaki (Northwestern University) and Igor Schapiro (Hebrew University) for their advice and help in setting up and using the BAGEL code.

■ REFERENCES

(1) Kukk, E.; Motomura, K.; Fukuzawa, H.; Nagaya, K.; Ueda, K. Molecular Dynamics of XFEL-Induced Photo-Dissociation, Revealed by Ion-Ion Coincidence Measurements. *Appl. Sci.* **2017**, *7*, 531.

(2) Erk, B.; et al. Imaging charge transfer in iodomethane upon x-ray photoabsorption. *Science* **2014**, *345*, 288−291.

(3) Takanashi, T.; et al. Ultrafast Coulomb explosion of a diiodomethane molecule induced by an X-ray free-electron laser pulse. *Phys. Chem. Chem. Phys.* **2017**, *19*, 19707−19721.

(4) Vager, Z.; Naaman, R.; Kanter, E. P. Coulomb Explosion Imaging of Small Molecules. *Science* **1989**, *244*, 426−431.

(5) Strasser, D.; Lammich, L.; Krohn, S.; Lange, M.; Kreckel, H.; Levin, J.; Schwalm, D.; Vager, Z.; Wester, R.; Wolf, a.; Zajfman, D. Two- and three-body kinematical correlation in the dissociative recombination of H3+. *Phys. Rev. Lett.* **2001**, *86*, 779−782.

(6) Itakura, R.; Liu, P.; Furukawa, Y.; Okino, T.; Yamanouchi, K.; Nakano, H. Two-body Coulomb explosion and hydrogen migration in methanol induced by intense 7 and 21 fs laser pulses. *J. Chem. Phys.* **2007**, *127*, 104306.

(7) Xu, H.; Okino, T.; Kudou, T.; Yamanouchi, K.; Roither, S.; Kitzler, M.; Baltuska, A.; Chin, S. L. Effect of laser parameters on ultrafast hydrogen migration in methanol studied by coincidence momentum imaging. *J. Phys. Chem. A* **2012**, *116*, 2686−2690.

(8) Posthumus, J. H. The dynamics of small molecules in intense laser fields. *Rep. Prog. Phys.* **2004**, *67*, 623−665.

(9) Frasinski, L. J.; Plumridge, J.; Posthumus, J. H.; Codling, K.; Taday, P. F.; Divall, E. J.; Langley, a. J. Counterintuitive alignment of H2 + in intense femtosecond laser fields. *Phys. Rev. Lett.* **2001**, *86*, 2541−2544.

(10) Livshits, E.; Baer, R. Time-dependent density-functional studies of the D2 Coulomb explosion. *J. Phys. Chem. A* **2006**, *110*, 8443−8450.

(11) Prabhudesai, V. S.; Lev, U.; Natan, A.; Bruner, B. D.; Diner, A.; Heber, O.; Strasser, D.; Schwalm, D.; Ben-Itzhak, I.; Hua, J. J.; Esry, B. D.; Silberberg, Y.; Zajfman, D. Tracing the photodissociation probability of H2+ in intense fields using chirped laser pulses. *Phys. Rev. A: At., Mol., Opt. Phys.* **2010**, *81*, 023401.

(12) Ibrahim, H.; Lefebvre, C.; Bandrauk, A. D.; Staudte, A.; Légaré, F. H2: The benchmark molecule for ultrafast science and technologies. *J. Phys. B: At., Mol. Opt. Phys.* **2018**, *51*, 042002.

(13) Runge, E.; Gross, E. K. U. Density functional theory for time dependent systems. *Phys. Rev. Lett.* **1984**, *52*, 997−1000.

(14) Send, R.; Furche, F. First-order nonadiabatic couplings from time-dependent hybrid density functional response theory: Consistent formalism, implementation, and performance. *J. Chem. Phys.* **2010**, *132*, 044107−12.

(15) Zhang, D.; Peng, D.; Zhang, P.; Yang, W. Analytic gradients, geometry optimization and excited state potential energy surfaces from the particle-particle random phase approximation. *Phys. Chem. Chem. Phys.* **2015**, *17*, 1025−1038.

(16) Adamowicz, L.; Laidig, W. D.; Bartlett, R. J. Analytical gradients for the coupled-cluster method. *Int. J. Quantum Chem.* **1984**, *26*, 245−254.

(17) Gauss, J.; Stanton, J. F. Analytic gradients for the coupled-cluster singles, doubles, and triples (CCSDT) model. *J. Chem. Phys.* **2002**, *116*, 1773−1782.

(18) Krylov, A. I. Equation-of-motion coupled-cluster methods for open-shell and electronically excited species: The Hitchhiker's guide to Fock space. *Annu. Rev. Phys. Chem.* **2008**, *59*, 433−462.

(19) Roos, B. O.; Taylor, P. R.; Sigbahn, P. E. a. A complete active space SCF method (CASSCF) using a density matrix formulated super-CI approach. *Chem. Phys.* **1980**, *48*, 157−173.

(20) Roos, B. O.; Linse, P.; Siegbahn, P. E. M.; Blomberg, M. R. A. A Simple Method for the Evaluation of the 2nd-Order Perturbation Energy from External Double-Excitations with a Casscf Reference Wavefunction. *Chem. Phys.* **1982**, *66*, 197−207.

(21) Corkum, P. B. Plasma Perspective on Strong-Field Multiphoton Ionization. *Phys. Rev. Lett.* **1993**, *71*, 1994−1997.

(22) Månsson, E. P.; Guénot, D.; Arnold, C. L.; Kroon, D.; Kasper, S.; Dahlström, J. M.; Lindroth, E.; Kheifets, A. S.; Huillier, A. L.; Sorensen, S. L.; Gisselbrecht, M. Double ionization probed on the attosecond timescale. *Nat. Phys.* **2014**, *10*, 207−211.

(23) Zhou, X.; Ranitovic, P.; Hogle, C. W.; Eland, J. H.; Kapteyn, H. C.; Murnane, M. M. Probing and controlling non-Born-Oppenheimer dynamics in highly excited molecular ions. *Nat. Phys.* **2012**, *8*, 232−237.

(24) Gagnon, E.; Ranitovic, P.; Tong, X.-M. M.; Cocke, C. L.; Murnane, M. M.; Kapteyn, H. C.; Sandhu, A. S. Soft X-ray-Driven Femtosecond Molecular Dynamics. *Science* **2007**, *317*, 1374−1378.

(25) Molloy, R. D.; Danielsson, A.; Karlsson, L.; Eland, J. H. Double photoionisation spectra of small molecules and a new empirical rule for double ionisation energies. *Chem. Phys.* **2007**, *335*, 49−54.

(26) Luzon, I.; Jagtap, K.; Livshits, E.; Lioubashevski, O.; Baer, R.; Strasser, D. Single-photon Coulomb explosion of methanol using broad bandwidth ultrafast EUV pulses. *Phys. Chem. Chem. Phys.* **2017**, *19*, 13488−13495.

(27) Streeter, Z. L.; Yip, F. L.; Lucchese, R. R.; Gervais, B.; Rescigno, T. N.; McCurdy, C. W. Dissociation dynamics of the water dication following one-photon double ionization. I. Theory. *Phys. Rev. A: At., Mol., Opt. Phys.* **2018**, *98*, 053429.

(28) Park, J. W.; Shiozaki, T. On-the-Fly CASPT2 Surface-Hopping Dynamics. *J. Chem. Theory Comput.* **2017**, *13*, 3676−3683.

(29) Shiozaki, T. BAGEL: Brilliantly Advanced General Electronic-structure Library. *WIREs Comput. Mol. Sci.* **2018**, *8*, No. e1331.

(30) Ekanayake, N.; et al. Mechanisms and time-resolved dynamics for trihydrogen cation (H3+) formation from organic molecules in strong laser fields. *Sci. Rep.* **2017**, *7*, 4703.

(31) Ando, T.; Shimamoto, A.; Miura, S.; Iwasaki, A.; Nakai, K.; Yamanouchi, K. Coherent vibrations in methanol cation probed by periodic H3+ ejection after double ionization. *Communications Chemistry* **2018**, *1*, 7.

(32) Eland, J. H. The origin of primary H3+ ions in mass spectra. *Rapid Commun. Mass Spectrom.* **1996**, *10*, 1560−1562.

(33) Ekanayake, N. H2 roaming chemistry and the formation of H3+ from organic molecules in strong laser fields. *Nat. Commun.* **2018**, *9*, 5186.

(34) De, S.; Rajput, J.; Roy, A.; Ghosh, P. N.; Safvan, C. P. Formation of H3+ due to intramolecular bond rearrangement in doubly charged methanol. *Phys. Rev. Lett.* **2006**, *97*, 213201.

(35) Mebel, A. M.; Bandrauk, A. D. Theoretical study of unimolecular decomposition of allene cations. *J. Chem. Phys.* **2008**, *129*, 224311.

(36) Polanyi, M. Zum Ursprung der chemischen Energie. *Eur. Phys. J. A* **1920**, *3*, 31−35.

(37) Dalitz, R. CXII. On the analysis of τ-meson data and the nature of the τ-meson. *Phil. Mag. Ser.* **1953**, *44*, 1068−1080.

(38) Strasser, D.; Lammich, L.; Kreckel, H.; Krohn, S.; Lange, M.; Naaman, A.; Schwalm, D.; Wolf, A.; Zajfman, D. Breakup dynamics

and the isotope effect in H3+ and D3+ dissociative recombination. *Phys. Rev. A: At., Mol., Opt. Phys.* **2002**, *66*, 032719.

(39) Laperle, C. M.; Mann, J. E.; Clements, T. G.; Continetti, R. E. Three-body dissociation dynamics of the low-lying rydberg States of H 3 and D3. *Phys. Rev. Lett.* **2004**, *93*, 153202.

(40) Bucksbaum, P. H.; Berrah, N. Brighter and faster: The promise and challenge of the x-ray free-electron laser. *Phys. Today* **2015**, *68*, 26−32.

(41) Reedy, D.; et al. Dissociation dynamics of the water dication following one-photon double ionization. II. Experiment. *Phys. Rev. A: At., Mol., Opt. Phys.* **2018**, *98*, 053430.

(42) Solstice Ace. https://www.spectra-physics.com/products/ultrafast-lasers/solstice-ace.

(43) Sutherland, J.; Christensen, E.; Powers, N.; Rhynard, S.; Painter, J.; Peatross, J. High harmonic generation in a semi-infinite gas cell. *Opt. Express* **2004**, *12*, 4430−4436.

(44) Salieres, P.; Ditmire, T.; Budil, K. S.; Perry, M. D.; L'Huillier, A. Spatial profiles of high-order harmonics generated by a femtosecond Cr:LiSAF laser. *J. Phys. B: At., Mol. Opt. Phys.* **1994**, *27*, L217−L222.

(45) Kandhasamy, D. M.; Albeck, Y.; Jagtap, K.; Strasser, D. 3D Coincidence Imaging Disentangles Intense Field Double Detachment of SF6-. *J. Phys. Chem. A* **2015**, *119*, 8076−8082.

(46) Aquilante, F.; Autschbach, J.; Carlson, R. K.; Chibotaru, L. F.; Delcey, M. G.; De Vico, L.; Fdez. Galván, I.; Ferré, N.; Frutos, L. M.; Gagliardi, L. a. Molcas 8: New capabilities for multiconfigurational quantum chemical calculations across the periodic table. *J. Comput. Chem.* **2016**, *37*, 506−541.

(47) Tully, J. C. Molecular-Dynamics with Electronic-Transitions. *J. Chem. Phys.* **1990**, *93*, 1061−1071.

(48) Vlaisavljevich, B.; Shiozaki, T. Nuclear energy gradients for internally contracted complete active space second-order perturbation theory: Multistate extensions. *J. Chem. Theory Comput.* **2016**, *12*, 3781−3787.

(49) Barbatti, M.; Ruckenbauer, M.; Plasser, F.; Pittner, J.; Granucci, G.; Persico, M.; Lischka, H. Newton-X: a surface-hopping program for nonadiabatic molecular dynamics. *WIREs Comput. Mol. Sci.* **2014**, *4*, 26−33.

DOI: 10.1021/acs.jpclett.9b00576
J. Phys. Chem. Lett. 2019, 10, 1361−1367